

We are IntechOpen, the world's leading publisher of Open Access books Built by scientists, for scientists

6,900

Open access books available

185,000

International authors and editors

200M

Downloads

Our authors are among the

154

Countries delivered to

TOP 1%

most cited scientists

12.2%

Contributors from top 500 universities



WEB OF SCIENCE™

Selection of our books indexed in the Book Citation Index
in Web of Science™ Core Collection (BKCI)

Interested in publishing with us?
Contact book.department@intechopen.com

Numbers displayed above are based on latest data collected.
For more information visit www.intechopen.com



Isoscape Analysis for Elucidating Relationships between Soil Redistribution and Soil Carbon Dynamics

Xia Li, Gregory McCarty and Sangchul Lee

Abstract

Isotopic tracers are useful for assessing linkages between soil movement and soil carbon dynamics in landscapes. Analyses of isotopes and comparison of isoscape (isotopic landscape) with observational data have been employed to investigate spatial distributions of isotopes, to test efficiencies of isotopic models, and to examine soil redistribution patterns and C dynamics. This chapter reviewed the application of natural (^7Be , ^{210}Pb) and anthropogenic fallout radionuclides (^{137}Cs , $^{239,240}\text{Pu}$), and C isotopes ($^{12,13,14}\text{C}$) in understanding mechanisms of soil redistribution and sedimentation. The chapter was organized to cover the formation, sources, and transport of these isotopes; how they are distributed and related to soil redistribution on C dynamics; and importance of their distribution (isoscapes) on investigating soil properties. We also provided a case study to demonstrate the feasibility of applying isotopes and isoscape modeling for understanding soil property variability in response to anthropogenic disturbance in a low-relief cropland field. Results demonstrated advantages of using ^{137}Cs and C isotopic signature ($\delta^{13}\text{C}$) to trace soil movements and C dynamics. Topography-based ^{137}Cs and C isoscape models were developed using light detection and ranging data (LiDAR) derived topographic metrics. The models successfully simulated the spatial patterns of ^{137}Cs inventory and $\delta^{13}\text{C}$ over an agricultural landscape and can benefit soil sedimentation and C dynamic studies in areas with limited observations.

Keywords: isotope analysis, isoscape, soil redistribution, soil carbon dynamics, dynamic replacement

1. Introduction

Soil redistribution (i.e., erosion and deposition) exerts a significant impact on the global carbon (C) cycle. Movement of soil particles could either redistribute soil C or change the C mineralization through disruption of soil aggregation, reaggregation of deposited soils, and deep burial of C-enriched sediments at depositional sites [1]. When soil erosion occurs, the surface concentrated and low-density proportions of sediments, such as soil organic carbon (SOC), are preferentially removed by runoff, wind, and/or tillage activities. A greater SOC enrichment ratio in eroded sediment is usually observed compared to its origin [2]. The eroded

sediment is either redistributed over a landscape or deposited at depressional sites. Therefore, investigation of soil redistribution and underlying mechanisms are needed for better understandings of the fate of soil C within the landscape.

Various methods have been developed to quantified soil redistribution. Before the 1990s, researchers mainly focused on understanding soil erosion by discerning changes in soil texture and chemical properties [3]. However, accuracy of this method was low, mainly because impacts of erosion on soil properties are complicated and vary with soil characteristics, soil depth, and local land use practices. Other studies adopted erosion prediction models, such as the USLE, WaTEM, and WEPP, to assess soil redistribution processes [4, 5]. Although these models reasonably estimated long-term mean erosion rates over large-scale, the estimates from the modeling are often mean redistribution rates at sites, model estimates from individual erosion events are too coarse to be linked to each soil samples to explain changes in soil properties [6].

The emergence of isotopic analysis allows researchers to accurately trace soil movement at locations, offering a potential way to quantify the impacts of soil erosion and deposition on soil properties. The isotopic tracer selection follows two criteria: (1) isotopes should be able to quickly and strongly absorbed by the soil; and (2) the variability in absorption to various textures or size is either minor or can be calculated [7]. A tracer can be uniformly distributed at first and then move with the soil movements, presenting mass variations between eroded and depositional sites.

This chapter examines the application of six widely used tracers, including anthropogenic fallout radionuclides/Cesium-137 (^{137}Cs), plutonium isotopes ($^{239,240}\text{Pu}$), natural fallout radionuclides Beryllium-7 (^7Be), Lead-210 (^{210}Pb), and C isotopes ($^{12,13,14}\text{C}$), in soil redistribution and C distribution studies. Objectives of this chapter are to (1) review impacts of soil redistribution on soil C dynamics; (2) summarize critical processes regulating the selected soil isotopes; (3) introduce the concept of isoscape and its applications in soil biogeochemical studies; and (4) provide discussion of isotopic and isoscape analyses for understanding of soil redistribution and carbon dynamics through a case study.

2. Soil redistribution impacts on soil C dynamics

The global soil inventory represents an important C pool (**Figure 1**) with a total of 1950 Gt C, accounting for 2.3 times the size of the atmospheric C pool (860 Gt C) and 3.5 times of the biotic C pool (550 Gt C) [8]. About 1750 Gt C of total soil C concentrates on land surface, where soil erosion and deposition processes are intense. The light and fine soil particles with high SOC content are preferentially removed by the erosion process and redistributed over a landscape or deposited at depressional sites. It was estimated that 75 Gt year⁻¹ of soil is removed by water and wind erosion [1], which contribute to 0.8–2.2 Gt year⁻¹ emission of C from land surface, and 2.5–3.9 Gt year⁻¹ of replaced C in soil [8].

Although researchers have increasingly recognized the importance of soil erosion and C dynamics on ecosystems, mechanisms of soil redistribution controls on soil C remains poorly understood. Some studies suggested negative effects of soil erosion on terrestrial C sequestration [9–11]. They provide an argument that excessive soil erosion can lead to losses of soil fertility, decreasing the plant and crop productivity [9]. Notably, the recently accelerated soil erosion due to agricultural activities has caused 2 billion ha of land being irreversibly degraded [1]. Plowing activity increases the possibility of soil organic matter within the plow layer to be exposed to anthropogenic and climatic perturbations, and thus accelerates SOC mineralization [11]. Furthermore, soil C mineralization in displaced soils can also

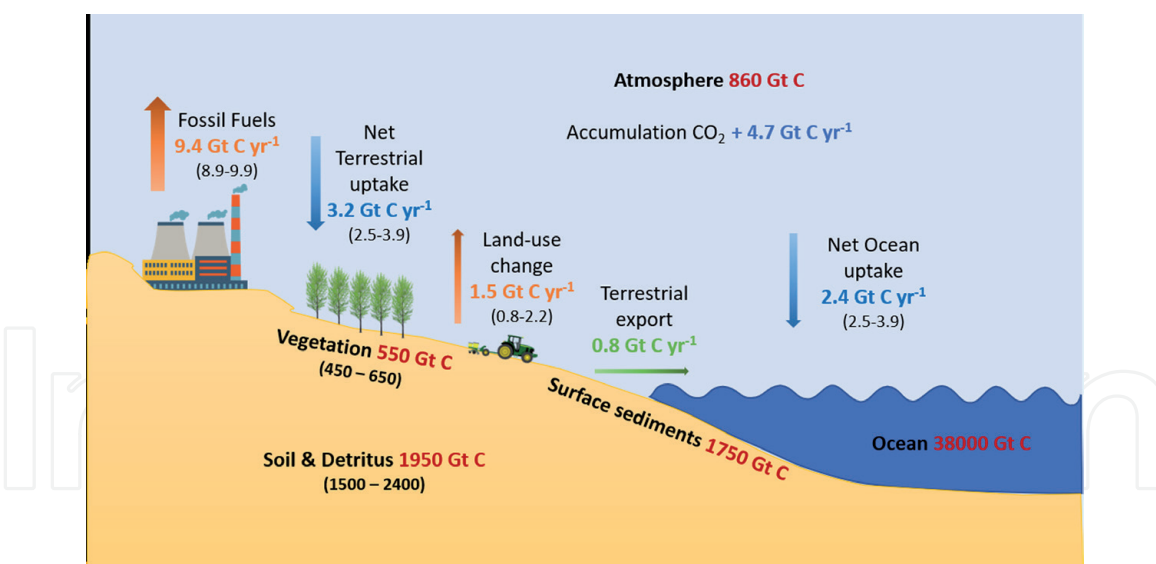


Figure 1.
 Global C budget for the decade 2008–2017. The C storage and dynamics were taken from Le Quéré et al. [8].

be stimulated as a result of the breakdown of soil aggregates by raindrop and runoff shearing forces that expose previously protected organic matters to oxidation [12]. It was estimated that more than 20% C emission was caused by mineralization of the displaced C [13].

On the contrary, arguments for positive impacts of soil redistribution on C storage support that redistribution of soil could increase C sequestration in terrestrial ecosystems [14–17]. SOC losses at the eroded sites could be dynamically replaced by litter input from plant regrowth and return of above- and below-ground biomass to soil and replenish the depleted SOC pool at eroded sites [18, 19]. The eroded SOC is subsequently buried and re-aggregated at depressional sites, protecting SOC from mineralization and thus increasing C sequestration [14, 20, 21]. Stallard [19] used a large set of scenarios estimated that the human-induced C burial is in the range of 0.6–1.5 Gt C year⁻¹ by terrestrial sedimentation.

3. Using isotopes in studies of soils and sediments

3.1 Anthropogenic fallout radionuclides

¹³⁷Cs is the most widely used isotope in geomorphic studies of water, wind and tillage erosion. As an anthropogenic radionuclide with a half-life of 30.2 years, ¹³⁷Cs was released globally into the environment due to radioactive fallout from nuclear weapon testing in the 1950s and 1960s and reached to land surface through wet and dry deposition (**Figure 2**). Additional ¹³⁷Cs fallout occurred because of the 1986 Chernobyl accident in the north of the Ukrainian SSR and the 2011 Fukushima accident in Japan. The overall amount of ¹³⁷Cs released from Fukushima was less than 15% of the amount from the Chernobyl accident [22]. The Fukushima accident added high amounts of ¹³⁷Cs to soils near the accident site, but the large-scale plume of radioactive fallout extended mainly over the Pacific Ocean which reduced the extent of terrestrial labeling. In contrast, Chernobyl is in the center of the European continent. The released fallout radionuclides significantly increased the ¹³⁷Cs amount in many European countries [22]. ¹³⁷Cs is chemically active and is rapidly and strongly absorbed by fine soil particles when it contacts with the soil. Vertical migration is slow and the majority of ¹³⁷Cs is retained in the upper 20 cm of the soil surface across the globe [23–25]. Once the soil is labeled by ¹³⁷Cs, chemical and

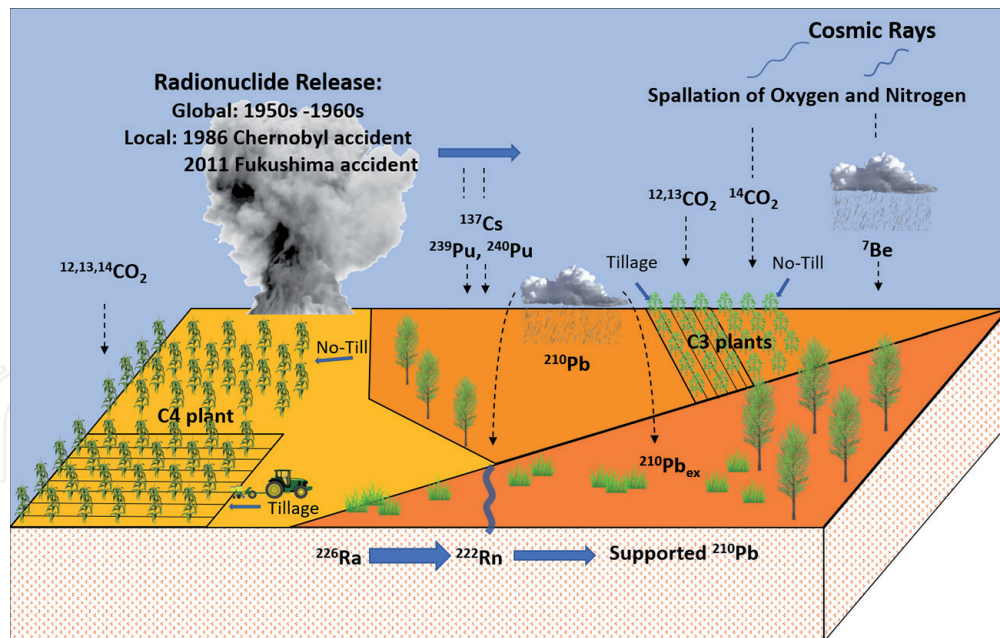


Figure 2.
Isotopes used as soil tracers in soil and sediment studies.

biological removal of ^{137}Cs is low. The ^{137}Cs concentration changes mainly result from physical processes in the top-layer soils, such as soil transport and deposition. Therefore, these characteristics make ^{137}Cs a useful tracer for quantifying of soil redistribution rates.

Previous investigations have reported strong and statistically significant correlations between ^{137}Cs and soil C [10, 26, 27]. However, because ^{137}Cs inventory is usually non-linearly correlated with soil redistribution, the correlations between ^{137}Cs inventory and soil C content are usually weaker than the correlations between soil redistribution process and SOC [6]. Consequently, instead of directly quantify SOC based on ^{137}Cs , most recent studies first converted ^{137}Cs measurements to soil redistribution rates, and then used the estimates to link to soil C content. Specifically, the application of ^{137}Cs measurements in soil redistribution and C dynamics mainly includes to (1) calculate soil redistribution at a point and link to soil properties of a soil sample from the same point [6, 28, 29]; (2) provide mean annual rate of soil redistribution over 60 years and reflect the erosion history of a site [10, 29]; and (3) present spatial patterns of soil erosion and deposition over the landscape [27, 30].

Because of the short half-life, ^{137}Cs concentration may drop below the detection limits quickly and limit use of this tracer in SOC investigations. Researchers are finding alternative tracers with longer half-lives for soil erosion investigation. Anthropogenic radionuclides of two major plutonium isotopes (^{239}Pu : half-life = 24,110 years and ^{240}Pu : half-life = 6561 years) are considered as potential alternatives for this purpose. Like ^{137}Cs , the Pu isotopes in soils are also mainly from nuclear weapon testing between the 1950s and 1960s following the 1986 Chernobyl accident. However, the isotopic composition of Chernobyl Pu ($^{240}\text{Pu}/^{239}\text{Pu}$ atom ratio: 0.37–0.41) presents higher ratios compared to Pu from nuclear testing ($^{240}\text{Pu}/^{239}\text{Pu}$ atom ratio = 0.180 ± 0.014), which can be used to distinguish Pu isotopes from the two sources [31]. Some researchers have argued that in soils with high organic matter, Pu might be preferentially absorbed by organic fractions with high molecular weight and potentially lead to a deep vertical migration [32, 33].

Considering the long half-life of Pu isotopes, increasing studies have explored the feasibility of using Pu isotopes in investigations of soils and sediments [34–36]. Schimmack et al. [37] found that the Chernobyl Pu could be a better tracer for soil redistribution detections in Bavaria, Germany, since spatial patterns of Pu agreed

better with soil mapping than that of ^{137}Cs . Similar conclusions were reached in several other studies, reporting more homogenous distributions of $^{239+240}\text{Pu}$ than ^{137}Cs in parts of Europe that were influenced by the Chernobyl accident [31, 38]. Thus, the isotopic composition variations may lead Pu isotopes to be a better choice than ^{137}Cs for tracing soil erosion. However, the feasibility of applying $^{239,240}\text{Pu}$ to soil erosion and soil C investigations still needs further testing because of its vertical migration and lateral transport by water, which may influence the quantification of soil redistribution [39, 40].

3.2 Natural radionuclides

^7Be is a natural radionuclide produced primarily through cosmic-ray spallation of oxygen and nitrogen nuclei in the stratosphere and troposphere. Unlike the anthropogenic radionuclides of ^{137}Cs and $^{239,240}\text{Pu}$, wet and dry deposition of ^7Be to the soil surface is continuous because of its natural origin [41]. The concentration of ^7Be in the soil decreases with increases in particle size [42]. Vertical migration was low for this isotope due to its relatively short half-life (half-life = 53.3 days). Wallbrink and Murray [42] found that most of soil ^7Be was accumulated in the top 20 mm regardless of soil types and surface cover conditions at two Australian sites.

Because of its short half-life, ^7Be has the potential to trace short-term soil redistribution. A number of studies have used this isotope to examine short-term soil erosion after heavy rain events, providing a basis for understanding sediment transported by dispersed overland flow [41–44]. Considering the lower vertical transport of ^7Be relative to ^{137}Cs and excess ^{210}Pb ($^{210}\text{Pb}_{\text{ex}}$), this isotope has been applied to discriminate vertical and horizontal erosion by combining with the other two isotopes [45, 46]. Ryken et al. [47] suggested correction factors related to particle size and variations in relaxation mass depth should be used to get precise estimates of ^7Be -derived soil redistribution rates. Li et al. [48] successfully applied ^7Be to quantify SOC sequestration changes caused by land-use and management activity.

Another natural isotope, Lead-210 (^{210}Pb) produced through the decay of gaseous Radon-222 (^{222}Rn) generated from the decay of Radium-226 (^{226}Ra) in the Uranium-238 (^{238}U) decay series. ^{226}Ra exists in soils and rocks. Most of ^{226}Ra decay to ^{210}Pb in situ, which is termed supported ^{210}Pb . Due to diffusion, a small portion of ^{226}Ra -derived ^{222}Rn enters to the atmosphere and subsequently introduces ^{210}Pb to the atmosphere. This kind of ^{210}Pb falls to land surface through wet and dry deposition and is termed unsupported or excess ^{210}Pb ($^{210}\text{Pb}_{\text{ex}}$). The $^{210}\text{Pb}_{\text{ex}}$ is strongly absorbed by fine soil particles and transports with soil movement. $^{210}\text{Pb}_{\text{ex}}$ fallout is continuous over time, which is like ^7Be , but its half-life (half-life = 22.3 years) is longer than ^7Be . Therefore, $^{210}\text{Pb}_{\text{ex}}$ has the potential to penetrate deeper soil layers (to 10 cm) than ^7Be [7, 23].

The use of $^{210}\text{Pb}_{\text{ex}}$ in soil and sediment studies has increased in recent decades. Due to the continuous fallout, $^{210}\text{Pb}_{\text{ex}}$ can be used to provide long-term soil redistribution rates. Meanwhile, unlike ^{137}Cs , $^{210}\text{Pb}_{\text{ex}}$ does not have below-detection-limit problems caused by medium-lived anthropogenic fallout radionuclides. In practice, two or more different fallout radionuclides can be used to understand the soil erosion history. $^{210}\text{Pb}_{\text{ex}}$ is combined with ^{137}Cs and/or ^7Be to provide soil redistribution records in the past 100 years. Several studies suggested that $^{210}\text{Pb}_{\text{ex}}$ and ^7Be can produce similar spatial patterns [45, 49], but differences resulting from different land uses could help sediment source identification [46, 50]. Increasing applications of $^{210}\text{Pb}_{\text{ex}}$ in C dynamic studies have been reported recently [10, 15, 51, 52]. Investigations have demonstrated that $^{210}\text{Pb}_{\text{ex}}$ is preferentially associated with SOC than ^{137}Cs , due to the stronger binding to the organic matter in soils [53, 54].

3.3 C isotopes

The origin of soil C isotopes (^{12}C , ^{13}C , and ^{14}C) is mainly from plant litter entering the soils. During photosynthesis, plant species absorb atmospheric carbon dioxide (CO_2), which consists of about 98.9% of $^{12}\text{CO}_2$, 1.1% of $^{13}\text{CO}_2$, and trace amount of $^{14}\text{CO}_2$ (1 part in trillion). ^{14}C is a natural radionuclide created primarily by the cosmic-ray spallation of nitrogen in the troposphere and the stratosphere. ^{14}C is a relatively stable radioactive isotope with a half-life of 5730 years [55]. This C isotope is assimilated during plant photosynthesis and entering soil through litter fall and commonly used for age dating.

Data on the stable C isotopes ^{12}C and ^{13}C are usually reported $\delta^{13}\text{C}$ representing deviation of measured ^{13}C from the established natural abundance with units of parts per thousand (‰). Variations in soil $\delta^{13}\text{C}$ values are controlled primarily by carbon input from plant litter. Due to isotopic discrimination by their photosynthetic enzymes and the regulation of stomatal diffusion resistance, $\delta^{13}\text{C}$ values in plants cover a wide range. Plants with C3 photosynthesis have $\delta^{13}\text{C}$ values in a range of -22 to -32‰ . Plants with C4 photosynthesis are less depleted in ^{13}C with higher $\delta^{13}\text{C}$ values ranging from -9 to -17‰ . After plant residues entering the soil, the $\delta^{13}\text{C}$ values may change slightly due to isotope fractionation during microbial decomposition.

Soil C isotopes can effectively detect soil redistribution and reflect soil C dynamics over the landscape. Because of the isotopic variability in different plant species, soil $\delta^{13}\text{C}$ has been successfully applied to distinguish eroded soil sources and to identify soil sources from different land use types [56, 57]. Furthermore, due to the significant difference of C isotopic ($\delta^{13}\text{C}$ and ^{14}C) values between surface soils and subsoils, scientists also utilized the isotopes to obtain a better understanding of the origins and age of eroded SOC [2, 57]. Trends of $\delta^{13}\text{C}$ and ^{14}C by soil depth can be used to reconstruct history of vegetation succession based on different isotopic compositions [55, 58]. Li et al. [29] used both $\delta^{13}\text{C}$ and ^{137}Cs to investigate soil C fate in an agricultural field under an annual crop rotation of soybean (*Glycine max* [L.] Merr.) and maize (*Zea mays* L.) which represent C3 and C4 crop types respectively. They found that only C3-derived SOC was highly correlated with soil redistribution rates. The results indicated that SOC from different plant species might have different responses to physical disturbances (i.e., erosion and deposition) and biogeochemical transformations such as SOC mineralization.

4. Use of isoscapes in studies of soils and sediments

The spatial and temporal features of isotopes in various environmental materials can be predicted using both landscape and biogeochemical models [59]. The term of isoscape was introduced in the 2000s to describe spatial patterns of isotopes produced by various quantitative models using several environmental variables as predictors [60, 61]. Now isoscape analyses are widely used as a tool to understand the biogeochemistry of landscapes under study. Applications of isoscapes on soils and sediments can be categorized into three groups:

1. Isotopes can be used as the baseline in modeling studies. With the help of a robust model, regional isotopes can be estimated from gridded environmental datasets. Isoscapes provide a powerful tool for probing the efficiencies of these prediction models [62];

2. Comparison of isotopic spatial patterns with observed soil organic C and nitrogen (N) is useful for investigating the impacts of soil redistribution on soil properties. Isoscapes can effectively reflect soil redistribution patterns across space, which can be used to better explain spatial variability of soil properties [29, 63, 64];
3. Soil isoscapes is also used in investigations of plant and animal isoscapes. For example, because the primary input of ^{12}C and ^{13}C to soil are from plant litter, maps of soil $\delta^{13}\text{C}$ isoscape could provide information related to the biogeography of C3 and C4 plants and their relative contributions to the atmospheric C sequestration [65].

5. Application of isotopic analysis in an agricultural field

5.1 Study area introduction

A case study is presented to demonstrate the application of isotopic analysis and isoscape modeling in investigation of soil redistribution and C dynamics in cropland. The study was conducted in an agricultural field in Walnut Creek Watershed (WCW), Iowa. The WCW is in a humid continental climatic zone with relatively flat terrain (**Figure 3a**). Representative soils are a poor-drained Nicollet (mesic Aquic Hapludolls) in the lowlands and well-drained Clarion (mesic Typic Hapludolls) in the uplands. The dominant land use type in the WCW is agriculture. More than 86% of the watershed is farmlands. Primary tillage practices in the watershed are chisel plowing in autumn and disking in spring. The directions of tillage depend on the farm management and field configuration. Most of the area followed the north-south or east-west tillage directions.

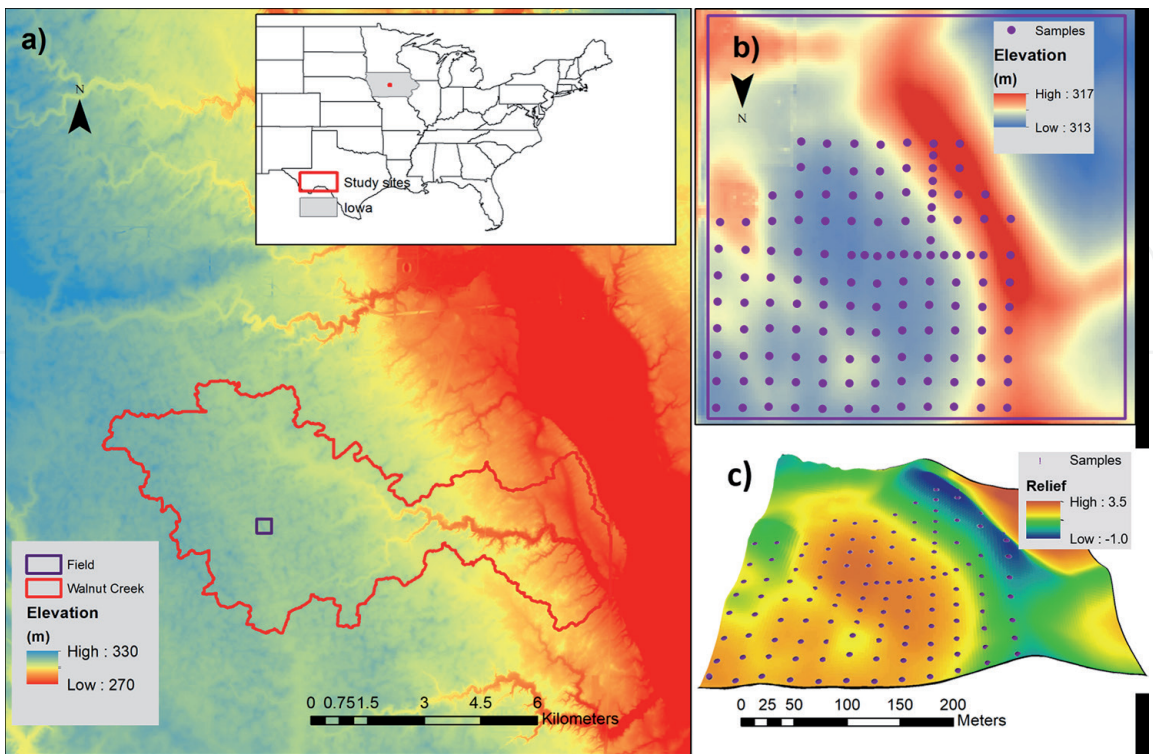


Figure 3. Elevation variability of (a) Walnut Creek Watershed (WCW) and (b) the cropland field, and (c) relief variability of the cropland field.

The studied cropland field is about 15 ha (**Figure 3b**). The maximum elevation change within a radius of 90 m is 4.5 m (**Figure 3c**). A C4–C3 crops rotation (i.e., maize-soybean) has been adopted in this area since 1957, which make this field an appropriate testbed for a detailed C isotope study assessing impacts of soil redistribution.

5.2 Methods

5.2.1 Sampling and laboratory analyses

Isotopes of ^{137}Cs , ^{12}C , and ^{13}C were measured in soil samples. A total of 119 locations were collected at grid nodes in a 25×25 m grid. A 9-sample and an 11-sample transects were set at an interval of 12.5 m within the grid (**Figure 2b and c**). We also selected four reference sites for estimating the baseline ^{137}Cs inventory. Three samples were collected from the top 30 cm of soil within a 1×1 m quadrat using a 3.2 cm diameter push probe at each location. All soil samples were oven dried and weighed for soil bulk density calculation.

SOC content was estimated as the difference between total C that was measured by a LECO CNS 2000 elemental analyzer and calcium C estimated using soil samples ashed in a furnace at 420°C . SOC content (%) was then converted to SOC density (kg m^{-2}) using soil bulk density.

The $^{13}\text{C}/^{12}\text{C}$ isotope ratio was measured using an isotope-ratio mass spectrometer (Europa Scientific Ltd., Crewe, England). The ratio was then combined with the laboratory reference that was calibrated against the international Pee Dee Belemnite (PDB) to estimated $\delta^{13}\text{C}$ related to PDB.

This study estimated the relative contribution of C3 and C4 crops using the following equations:

$$F_{C4} = \frac{\delta^{13}\text{C} - \delta^{13}\text{C}_{C3}}{\delta^{13}\text{C}_{C4} - \delta^{13}\text{C}_{C3}} \quad (1)$$

$$F_{C3} = 1 - F_{C4} \quad (2)$$

where F_{C4} and F_{C3} are contribution fraction of C4- and C3- derived SOC, respectively. $\delta^{13}\text{C}_{C3}$ and $\delta^{13}\text{C}_{C4}$ are the isotopic signatures for C3 and C4 crops. According to the literature review, the average $\delta^{13}\text{C}_{C3}$ and $\delta^{13}\text{C}_{C4}$ values for soybean and maize are -27 and -12% . Therefore, we used these two values to obtain the likelihood C3- and C4-derived SOC in this field.

To measure ^{137}Cs , gamma-ray analysis was performed using a Canberra Genie-2000 Spectroscopy System. Original unit of ^{137}Cs concentration was becquerels per gram (Bq g^{-1}), and this unit was subsequently converted to becquerels per square meter (Bq m^{-2}) using soil bulk density. The baseline ^{137}Cs inventory estimated from reference sites and the ^{137}Cs inventory of sampling sites were used to calculate ^{137}Cs -derived soil redistribution rates using the Mass Balance model I developed by Walling et al. [66]. In this study, the baseline ^{137}Cs inventory was 2657 Bq m^{-2} . Sites with higher ^{137}Cs inventories than the baseline were considered as depositional sites; while sites with lower ^{137}Cs inventories were referred as eroded sites.

Additional sampling and laboratory analyses details are given in Li et al. [29].

5.2.2 Historic orthophoto interpretation

Historic orthophotos in the 1950s and 2002 were obtained from the Iowa geographic map server (<http://ortho.gis.iastate.edu/>) to visualize soil movement. The

surface soil layer was referred as mollic epipedon formed under grass vegetation that dominated this area prior to the 1850s. The mollic epipedon has a characteristic black color and contains a high amount of soil organic matter. Therefore, the black mollic epipedon can be visually identified in the historic orthophoto, serving as an indicator for soil erosion and deposition investigation after the 1850s. In this study, greyness values were derived from the orthophotos to quantify the intensity of black carbon signal related to the mollic epipedon. The values were compared to ^{137}Cs -derived soil redistribution rates to assess the appropriateness of using ^{137}Cs to trace soil movement in this low-relief cropland.

5.2.3 Terrain analyses

Topographic metrics used to describe features of the landscape were generated from the light detection and ranging (LiDAR)—derived 3 m digital elevation model (DEM). Fourteen topographic metrics were developed, including slope, profile curvature (P_Cur), plan curvature (Pl_Cur), general curvature (G_Cur), flow accumulation (FA), topographic relief [topographic relief principal components (TRPCs) and topographic relief factors (TRFAs)], positive topographic openness (PTO), downslope index (DI), flow path length (FPL), catchment area (CA), topographic wetness index (TWI), stream power index (SPI), upslope slope (UpSl), and flow length factor (LS) (**Table 1**). Before calculating topographic metrics, the DEM was filtered twice through a low pass 3-by-3 filter. Maps of slope, P_Cur, Pl_Cur, G_Cur, PTO, DI, FPL, CA, TWI, SPI, UpSl, and LS were developed by the System for Automated Geoscientific Analyses (SAGA) v. 2.2.5 [67]. FA map was generated with ArcGIS.

For TRPCs, a series of topographic relief maps with different spatial scales were generated. The topographic relief shows the elevation differences between the filtered DEM and a maximum elevation map showing a continuous surface of maximum elevation within a specific area/radius. Seven relief images were generated from seven maximum elevation maps using radiuses of 7.5, 15, 30, 45, 60, 75, and 90 m. Principal component analysis (PCA) was conducted to convert the seven reliefs to seven independent components, and the first two topographic relief principal components (TRPC1 and TRPC2) were selected for further analysis. Similarly, varimax rotated Factor Analysis (FAn) was used and the first two TRFA1 and TRFA2 were selected. The detailed topographic processing can be found in Li et al. [68].

5.2.4 Statistical analysis and model calibration

Duncan's multiple range tests ($p \leq 0.05$) were applied to test the mean differences of soil texture, soil SOC density, $\delta^{13}\text{C}$, ^{137}Cs inventory, ^{137}Cs -derived soil redistribution rates, and likelihood C3- and C4-derived SOC density between eroded and depositional sites. Topographic metrics of the 128 sampling locations were extracted from the DEM-derived topographic metric maps. Because some of the topographic metrics were highly correlated, PCA and varimax rotated FAn were applied to convert to mutually independent topographic combinations to reduce errors caused by collinearity between the metrics. The first six principal components (TPCs) and the first six factors (TFAs) were selected to develop isoscape models.

Models including the multiple linear regression (MLR) combined with principal component analysis (MLR-PCA) and MLR combined with factor analysis (MLR-FAn) models for SOC, ^{137}Cs , and $\delta^{13}\text{C}$ were developed using stepwise linear regression with the "leave-one-out" cross-validation. We randomly selected 70% samples

Variables	Definition	Generating method
Slope (radian)	An angle between a tangent and a horizontal plane at a given point	Slope, aspect, curvature module, SAGA
P_Cur (m ⁻¹)	Curvature of the surface in the direction of the steepest slope	
Pl_Cur (m ⁻¹)	Curvature in a horizontal plane	
G_Cur (m ⁻¹)	Curvature of the surface itself	
FA (m ²)	Land area that contributes surface water to an area in which water accumulates	ArcGIS
TRPC and TRFA	Topographic relief is elevation difference between the highest point over an area and a given location. TRPC/TRFA is topographic relief principal component/Topographic relief factor and is generated by several reliefs that are at different spatial-scales using principal component analysis/factor analysis	ArcGIS
PTO (radian)	An angular measure of the relation between surface relief and horizontal distance	Topographic openness module, SAGA
DI (radian)	Head differences along a flow path	Downslope distance gradient module, SAGA
FPL (m)	Maximum distance of water flow to a point in the catchment	Flow path length module, SAGA
CA (m ²)	Area draining to catchment outlet	SAGA wetness index module, SAGA
TWI	Frequencies and duration of saturated conditions	
SPI	Erosive power of overland flow	Stream power index module, SAGA
UpSl (radian)	Mean slope of upslope area	LS-factor (field based) module, SAGA
LS	Erosive power of the terrain	
<i>P_Cur, Pl_Cur, and G_Cur are profile curvature, plan curvature and general curvature, respectively; TRPC and TRFA are topographic relief principal components and topographic relief factors, respectively; PTO is positive topographic openness; DI is downslope index; CA is catchment area; TWI is topographic wetness index; SPI is stream power index; Upsl is upslope slope; LS is slope length factor.</i>		

Table 1.
Definitions and generating methods of selected topographic metrics.

as training dataset used for model calibration and 30% samples as testing dataset for model validation. Three criteria were used to evaluate model efficiencies. The three criteria are the adjusted coefficient of determination (R_{adj}^2), the Nash-Sutcliffe efficiency (NSE), and ratio of the root mean square error (RMSE) to the standard deviation of measured data (RSR). Usually, the model performance is considered satisfactory when NSE is larger than 0.5 and RSR is smaller than 0.7 [69].

5.3 Results and discussion

5.3.1 Soil redistribution impacts on C dynamics

Distribution of mollic epipedon, characterized by presence of black soil organic matter, reflected historical soil movement (**Figure 4**). The top-layer black soil

presumably blanketed the prairie landscape and was then transported by water and tillage from eroded upslope to downslope locations. This phenomenon can be observed from the higher mollic epipedon in the concave than the convex locations in the 1950s and likely more consolidated by 2002. The significant correlations between greyness values and ^{137}Cs -derived soil redistribution rate suggested that ^{137}Cs inventory can effectively reflect the soil redistribution process in this field.

The cropland experienced a general soil export as indicated by a negative mean ^{137}Cs -derived soil redistribution rate ($-0.51 \pm 2.09 \text{ kg m}^{-2} \text{ year}^{-1}$, **Table 2**). Specifically, about 81 locations were identified as eroded sites with negative soil redistribution rates (mean: $-1.72 \pm 1.38 \text{ kg m}^{-2} \text{ year}^{-1}$) and 47 locations were depositional sites with positive soil redistribution rates (mean: $1.57 \pm 1.32 \text{ kg m}^{-2} \text{ year}^{-1}$). SOC density exhibited a similar spatial pattern as soil redistribution rates with a higher mean value at depositional than eroded sites. The mean SOC density at depositional sites was about 1.70 times of that at eroded sites.

A strong and significant correlation was observed between ^{137}Cs -derived redistribution rates and SOC density ($r^2 = 0.667$, **Figure 5a**), which demonstrated that ^{137}Cs inventories can capture spatial patterns of SOC. The positive relationship between soil redistribution and SOC density is mainly caused by the preferential removal of C during soil erosion. The SOC is primarily concentrated on the topsoil layer and is prone to transport through runoff, wind, and tillage activities due to its low density. Silt and clay density that were enriched in SOC showed lower values at eroded sites than depositional sites could also provide evidence for the preferential movement of low-density particles [29].

Note that SOC mineralization and dynamic replacement can complicate impacts of soil redistribution on SOC. On the one hand, SOC mineralization highly depends on soil moisture conditions. Impacted by soil texture, soil moisture is commonly lower at upslope areas than low-lying areas. Our study area also showed similar spatial patterns in soil texture over the landscape [29]. The decreased fine particles

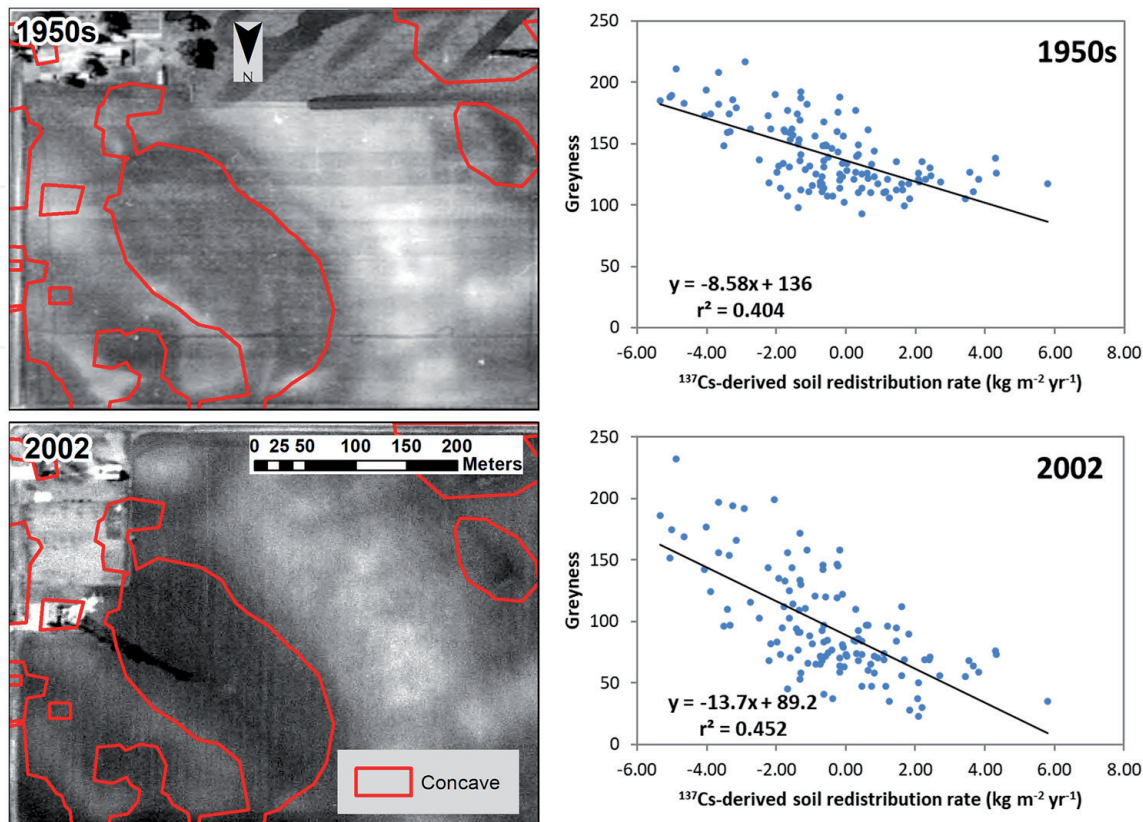


Figure 4.
Historic orthophotos and bivariate relationships between greyness and ^{137}Cs inventory in the 1950s and 2002.

	N	SOC	$\delta^{13}\text{C}$	^{137}Cs	SR	C3	C4
Erosion	81	759 (246) b [†]	-19.6 (2.05) a	1791 (532) b	-1.72 (1.38) b	396 (202) b	363 (131) a
Deposition	47	1292 (259) a	-21.9 (1.52) b	3547 (769) a	1.57 (1.32) a	852.2 (226) a	440 (152) a
All	128	956 (359)	-20.4 (2.16)	2435 (1056)	-0.51 (2.09)	565 (305)	391 (143)

N is the number of samples.
[†]Letters (a and b) estimate based on Duncan's multiple range tests. There are no significant ($p < 0.05$) differences for a parameter with the same letter.

Table 2.
Means (standard deviations) of soil organic carbon (SOC, kg m^{-2}), isotopic signature ($\delta^{13}\text{C}$, ‰), Cesium-137 (^{137}Cs) inventory (Bq m^{-2}), ^{137}Cs -derived soil redistribution (SR, $\text{kg m}^{-2} \text{ year}^{-1}$), and likelihood C3- and C4-derived SOC density (kg m^{-2}) in the cropland field.

(clay and silt) can reduce soil water retention, decrease aggregate stability, and increase oxygen concentration, accelerating SOC mineralization and further exacerbate SOC depletion in eroded areas [12]. On the other hand, the depleted SOC pool can be dynamically replaced by the continually deposited SOC from litter decomposition of above- and below-ground biomass. The net sequestration of carbon is not always linear over time because rates of replaced carbon at eroded sites depend on management history that may vary with time [18].

Values of $\delta^{13}\text{C}$ showed opposite spatial patterns with SOC and ^{137}Cs -derived soil redistribution rates with a higher mean value of $\delta^{13}\text{C}$ at eroded than depositional sites. The mean $\delta^{13}\text{C}$ value at the eroded sites was $-19.6 \pm 2.05\%$; while the $\delta^{13}\text{C}$ value at the depositional sites was $-21.9 \pm 1.52\%$. The higher mean $\delta^{13}\text{C}$ value at eroded sites indicated that the eroded sites were less depleted for ^{13}C and exhibited stronger C4 vegetation characteristics than depositional sites. The $\delta^{13}\text{C}$ value variability over this space possibly resulted from dynamic replacement. Our study area was dominated by prairie vegetation with strong C3 vegetation characteristics before the 1850s. After that, C4-derived SOC was introduced as a new SOC formation into the soil due to the widespread maize cultivation [70]. The new soil C (C4-derived SOC) replaced 50% of native soil C (C3-derived SOC) at eroded sites and 30% at depositional sites till 2002 when sampled.

According to the calculations of the relative contributions of C3 and C4 crops to the SOC, the C3-derived SOC density showed a significant difference between eroded ($396 \pm 202 \text{ kg m}^{-2}$) and depositional sites ($852 \pm 226 \text{ kg m}^{-2}$) while the C4-derived SOC density varied insignificantly (Table 2, eroded: $363 \pm 131 \text{ kg m}^{-2}$; depositional: $440 \pm 152 \text{ kg m}^{-2}$). C3-derived SOC density was positively related to ^{137}Cs -derived soil redistribution rates with a coefficient of determination of 0.65 (Figure 5b). In contrast, C4-derived SOC density was not strongly related

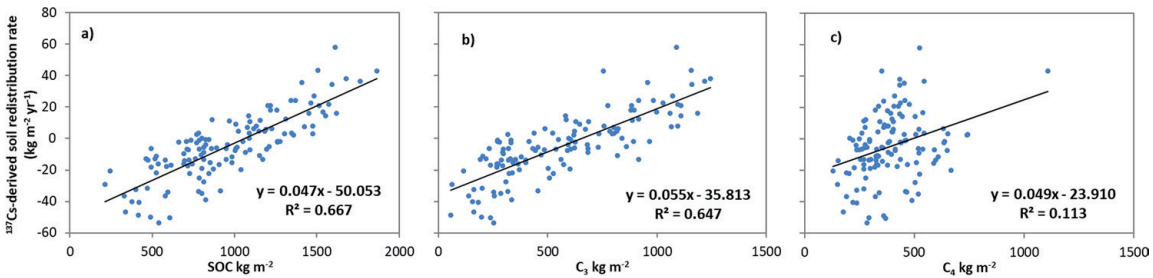


Figure 5.
Bivariate relationships between ^{137}Cs -derived soil redistribution rates and (a) SOC density, (b) C3- and (c) C4-derived SOC density.

to soil redistribution rates (**Figure 5c**). The different responses to soil erosion may be related to chemical compounds contained in the C3- and C4-derived SOC. Generally, liable compounds that are high in C4 crop residues are less depleted in ^{13}C than lignin-based compounds that are high in C3 crop residues [71]. Therefore, C4-derived SOC may largely be found in the mollic epipedon and be significantly affected by C mineralization, resulting in a decreased correlation with patterns of soil movement. In contrast, the more recalcitrant SOC in soil with strong C3 vegetation characteristics would be less influenced by C mineralization because it contains higher amount of stable lignin-based compounds. Therefore, the variability in C3 signature of soil C would more strongly correlate with patterns of soil redistribution.

5.3.2 Isoscape model development

Based on the derived topographic metrics, the first six TPCs and six TFAs were selected to construct independent topographic variables. The metrics with the highest absolute loadings for the first six TPCs were TWI, TRPC2, FA, FPL, DI, and CA. Therefore, the TPCs 1, 2, 3, 4, 5, and 6 were associated with soil wetness, flow acceleration, runoff volume, flow velocity, downslope dispersal, and water volume, respectively [72]. The highest absolute loadings in the six TFAs were Upsl, G_Cur, Pl_Cur, FPL, CA, and DI, which were associated with upslope flow velocity, flow acceleration, flow convergence and flow divergence, flow velocity, water volume, and downslope dispersal, respectively.

SOC and isoscape models of $\delta^{13}\text{C}$ and ^{137}Cs were developed using MLR-PCA and MLR-FAn (**Table 3**). Both types of models (MLR-PCA and MLR-FAn) presented satisfactory efficiencies during model calibration, but more independent variables were selected in MLR-FAn models. For SOC simulation, the MLR-PCA model selected four components with a R^2_{adj} of 0.668, an NSE of 0.682, and an RSR of 0.563. The MLR-FAn model exhibited higher R^2_{adj} and NSE values and a lower RSE value than MLR-PCA SOC model. In contrast, for ^{137}Cs inventory and $\delta^{13}\text{C}$ simulations, similar R^2_{adj} values were observed between the two types of models, but the MLR-FAn models showed higher NSE and RSR values, which suggested that the ^{137}Cs and $\delta^{13}\text{C}$ values derived from MLR-FA models were less deviated from the corresponding observed values.

Model		R^2_{adj}	NSE	RSR
MLR-PCA				
SOC	$949-119\text{TPC1} + 86.9\text{TPC5} + 21.4\text{TPC2} + 37.2\text{TPC4}^\dagger$	0.668	0.682	0.563
^{137}Cs	$2466-327\text{TPC1} + 240\text{TPC5}$	0.597	0.606	0.628
$\delta^{13}\text{C}$	$-20.3 + 0.677\text{TPC1} + 0.250\text{TPC3} + 0.181\text{TPC2}$	0.614	0.626	0.611
MLR-FAn				
SOC	$950 + 189\text{TFA4}-147\text{TFA2}-112\text{TFA1} + 88.9\text{TFA6} + 82.1\text{TFA3} + 50.2\text{TFA5}$	0.663	0.686	0.560
^{137}Cs	$2459 + 447\text{TFA4} + 306\text{TFA3}-346\text{TFA1} + 316\text{TFA6}-301\text{TFA2} + 150\text{TFA5}$	0.587	0.615	0.621
$\delta^{13}\text{C}$	$-20.3 + 1.26\text{TFA1} + 0.717\text{TFA2}-0.741\text{TFA4}-0.406\text{TFA6}-0.317\text{TFA5}$	0.614	0.635	0.604

[†]The order of variables is based on the stepwise selection steps. TPC and TFA are topographic principal component and topographic factor, respectively.

Table 3.
Topography-based models for soil organic carbon (SOC), cesium-137 (^{137}Cs), and isotopic signature ($\delta^{13}\text{C}$) in the cropland field.

Although both types of models reasonably matched up with observations during model calibration, the MLR-PCA models had better performance in predictions than the MLR-FAn models when applied to the test dataset. Predicted SOC explained 62.0% variability in observed SOC using MLR-PCA model. The values of NSE and RSR were 0.612 and 0.622, respectively. MLR-PCA ^{137}Cs and $\delta^{13}\text{C}$ models also had satisfactory performance with NSE values larger than 0.5 and RSR values smaller than 0.7. The R^2 for ^{137}Cs and $\delta^{13}\text{C}$ prediction were 0.713 and 0.509, respectively. In contrast, all the MLR-FAn models presented lower efficiencies in predicting target variables. Especially for the $\delta^{13}\text{C}$, the NSE value was smaller than 0.5 and RSR value was larger than 0.7 when compared MLR-FAn predictions with observations.

The lower efficiencies of the MLR-FAn models than the MLR-PCA models may be caused by model over-fitting. PCA considers all the variance in the independent variables, including unique, error and shared variance during synthetic variable construction; while FAn only considered and presented the shared variance in the factor matrix. Therefore, differences exist during development of MLR-PCA and MLR-FAn models. In this case study, although these two types of models had similar performance during model calibration using training datasets, increased number of parameters in MLR-FAn models may increase model error using validation datasets with general decrease in model stability, leading to low accuracies during extrapolating prediction points to external sample sets [73].

The spatial patterns of SOC density, ^{137}Cs inventory, and $\delta^{13}\text{C}$ were generated using MLR-PCA models (**Figure 6**). SOC density showed a similar spatial variability as ^{137}Cs inventories, which is consistent with the strong correlations between the SOC density and ^{137}Cs -derived soil redistribution rate (**Figure 5a**). Both variables had high values in depressions and low values in ridge and sloping areas. For $\delta^{13}\text{C}$, an opposite pattern was observed with low values in concave landscapes and high values in convex landscapes.

The high model efficiencies demonstrated the feasibility of using topography-based isoscape MLR-PCA models for investigating the spatial variability of isotopes. Although limitations may exist due to unaccounted topographic variables and environmental impactors, such as variance in tillage activities, the DEM-derived topography-based models provide a cost-effective method for isoscape mapping, effectively reflecting

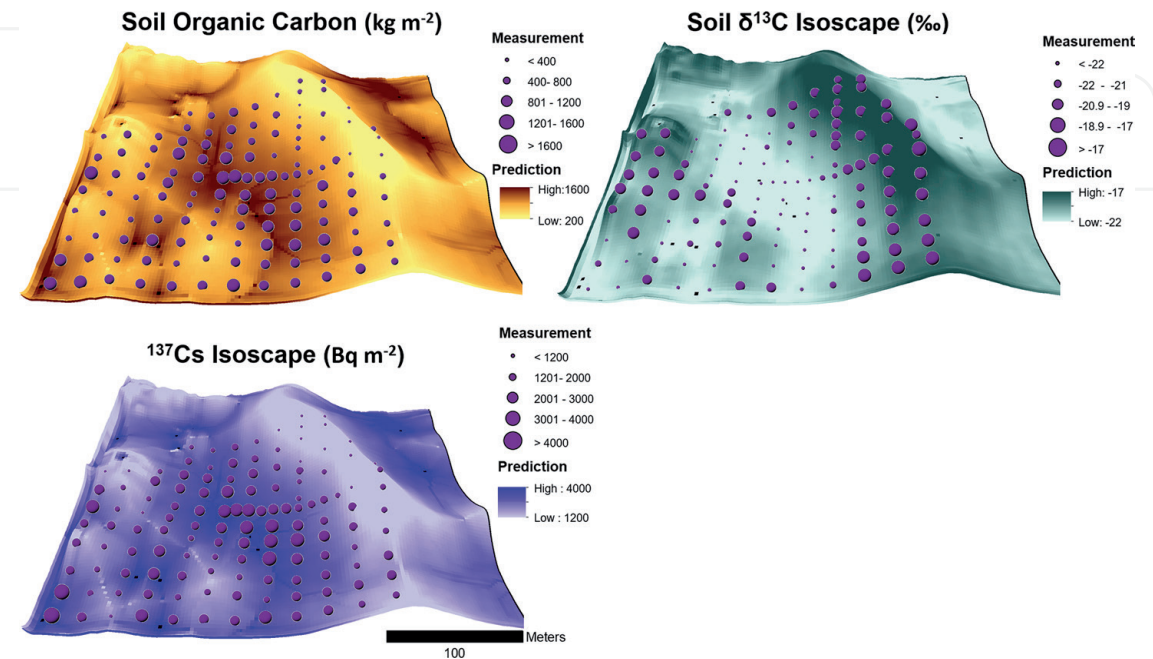


Figure 6. Spatial patterns of SOC density, ^{137}Cs inventory, and $\delta^{13}\text{C}$ in the study field.

redistribution patterns of soil and spatial patterns of SOC over the landscape [28, 74, 75]. These models can also benefit investigations in regions with limited access to ground measurements. The recently increased availability of the fine-resolution LiDAR data can further improve the model applicability, allowing for scaling of in situ isotopic simulations from field scale to isoscape mapping at watershed or regional scales.

6. Conclusions

Soil isotopes can effectively trace soil redistribution and SOC dynamics. This chapter reviewed the application of natural (^7Be , ^{210}Pb), anthropogenic fallout radionuclides (^{137}Cs , $^{239,240}\text{Pu}$), and C isotopes ($^{12,13,14}\text{C}$) in understanding soil erosion and deposition at different spatial and temporal scales. The case study demonstrated that ^{137}Cs and C isotopes could be employed to understand soil movement and C dynamics. SOC density showed high consistency with ^{137}Cs -derived soil redistribution rate, suggesting significant spatial impacts of soil movement on SOC. $\delta^{13}\text{C}$ provided further support of the importance of dynamic replacement on soil C dynamics in this area. Topography-based isoscape models were developed and effectively reconstructed the spatial variability in ^{137}Cs inventory and $\delta^{13}\text{C}$ over the landscape. The isoscape maps of ^{137}Cs and $\delta^{13}\text{C}$ were in general agreement with the spatial pattern of SOC density. Based on such results, we conclude that isotopic and isoscape analysis could provide valuable insights into soil movement and C studies.

Acknowledgements

This research was supported by the USDA Natural Resources Conservation Service in association with the Wetland Component of the National Conservation Effects Assessment Project (NRCS 67-3A75-13-177).

Conflict of interest


No conflict of interest exists relative to information presented in this chapter.

Author details

Xia Li, Gregory McCarty* and Sangchul Lee
Hydrology and Remote Sensing Laboratory, USDA-ARS, Beltsville, MD, USA

*Address all correspondence to: greg.mccarty@usda.gov

IntechOpen

© 2019 The Author(s). Licensee IntechOpen. This chapter is distributed under the terms of the Creative Commons Attribution License (<http://creativecommons.org/licenses/by/3.0>), which permits unrestricted use, distribution, and reproduction in any medium, provided the original work is properly cited. 

References

- [1] Lal R. Soil erosion and the global carbon budget. *Environment International*. 2003;**29**(4):437-450. DOI: 10.1016/S0160-4120(02)00192-7
- [2] Nadeu E, Berhe AA, De Vente J, Boix-Fayos C. Erosion, deposition and replacement of soil organic carbon in Mediterranean catchments: A geomorphological, isotopic and land use change approach. *Biogeosciences*. 2012;**9**(3):1099-1111. DOI: 10.5194/bg-9-1099-2012
- [3] Larson WE, Pierce FJ, Dowdy RH. The threat of soil erosion to long-term crop production. *Science*. 1983;**219**(4584):458-465. DOI: 10.1126/science.219.4584.458
- [4] Amore E, Modica C, Nearing MA, Santoro VC. Scale effect in USLE and WEPP application for soil erosion computation from three Sicilian basins. *Journal of Hydrology*. 2004;**293**(1-4):100-114. DOI: 10.1016/j.jhydrol.2004.01.018
- [5] Schumacher JA, Kaspar TC, Ritchie JC, Schumacher TE, Karlen DL. Identifying spatial patterns of erosion for use in precision conservation. *Journal of Soil and Water Conservation*. 2005;**60**(6):355-362
- [6] Du P, Walling DE. Using ^{137}Cs measurements to investigate the influence of erosion and soil redistribution on soil properties. *Applied Radiation and Isotopes*. 2011;**69**(5):717-726. DOI: 10.1016/j.apradiso.2011.01.022
- [7] Matisoff G, Whiting PJ. Measuring soil erosion rates using natural (^7Be , ^{210}Pb) and anthropogenic (^{137}Cs , $^{239,240}\text{Pu}$) radionuclides. In: *Handbook of Environmental Isotope Geochemistry*. Berlin: Springer; 2011. pp. 487-519. DOI: 10.1007/978-3-642-10637-8
- [8] Le Quéré C, Andrew RM, Friedlingstein P, Sitch S, Hauck J, Pongratz J, et al. Global carbon budget 2018. *Earth System Science Data*. 2018;**10**:2141-2194. DOI: 10.5194/essd-8-605-2016
- [9] Kosmas C, Gerontidis S, Marathianou M, Detsis B, Zafirou T, Nan Muysen W, et al. The effects of tillage displaced soil on soil properties and wheat biomass. *Soil and Tillage Research*. 2001;**58**(1-2):31-44. DOI: 10.1016/S0167-1987(00)00175-6
- [10] Li Y, Zhang QW, Reicosky DC, Lindstrom MJ, Bai LY, Li L. Changes in soil organic carbon induced by tillage and water erosion on a steep cultivated hillslope in the Chinese loess plateau from 1898-1954 and 1954-1998. *Journal of Geophysical Research-Biogeosciences*. 2007;**112**(1):1-10. DOI: 10.1029/2005JG000107
- [11] Martinez-Mena M, Lopez J, Almagro M, Boix-Fayos C, Albaladejo J. Effect of water erosion and cultivation on the soil carbon stock in a semiarid area of South-East Spain. *Soil and Tillage Research*. 2008;**99**(1):119-129. DOI: 10.1016/j.still.2008.01.009
- [12] Wang X, Cammeraat ELH, Cerli C, Kalbitz K. Soil aggregation and the stabilization of organic carbon as affected by erosion and deposition. *Soil Biology and Biochemistry*. 2014;**72**:55-65. DOI: 10.1016/j.soilbio.2014.01.018
- [13] Polyakov VO, Lal R. Soil erosion and carbon dynamics under simulated rainfall. *Soil Science*. 2004;**169**(8):590-599. DOI: 10.1097/01.ss.0000138414.84427.40
- [14] Van Oost K, Govers G, De Gryze S, Six J, Harden JW, Ritchie JC, et al. The impact of agricultural soil erosion

on the global carbon cycle. *Science*. 2007;**318**(5850):626-629

[15] McCarty GW, Pachepsky Y, Ritchie J. Impact of sedimentation on wetland carbon sequestration in an agricultural watershed. *Journal of Environmental Quality*. 2009;**38**(2):804-813. DOI: 10.2134/jeq2008.0012

[16] McCarty GW, Ritchie JC. Impact of soil movement on carbon sequestration in agricultural ecosystems. *Environmental Pollution*. 2002;**116**(3):423-430. DOI: 10.1016/S0269-7491(01)00219-6

[17] Berhe AA, Harden JW, Torn MS, Harte J. Linking soil organic matter dynamics and erosion-induced terrestrial carbon sequestration at different landform positions. *Journal of Geophysical Research – Biogeosciences*. 2008;**113**(4):1-12. DOI: 10.1029/2008JG000751

[18] Harden JW, Sharpe JM, Parton WJ, Ojima DS, Fries TL, Huntington TG, et al. Dynamic replacement and loss of soil carbon on eroding cropland. *Global Biogeochemical Cycles*. 1999;**13**(4):885-901. DOI: 10.1029/1999GB900061

[19] Stallard RF. Terrestrial sedimentation and the carbon cycle: Coupling weathering and erosion to carbon burial. *Global Biogeochemical Cycles*. 1998;**12**(2):231-257. DOI: 10.1029/98GB00741

[20] Lal R. Soil erosion and carbon dynamics. *Soil and Tillage Research*. 2005;**81**(2):137-142. DOI: 10.1016/j.still.2004.09.002

[21] Van Oost K, Govers G, Quine TA, Heckrath G, Olesen JE, De Gryze S, et al. Landscape-scale modeling of carbon cycling under the impact of soil redistribution: The role of tillage

erosion. *Global Biogeochemical Cycles*. 2005;**19**(4):1-13. DOI: 10.1029/2005GB002471

[22] Steinhäuser G, Brandl A, Johnson TE. Comparison of the Chernobyl and Fukushima nuclear accidents: A review of the environmental impacts. *Science of the Total Environment*. 2014;**470-471**:800-817. DOI: 10.1016/j.scitotenv.2013.10.029

[23] Doering C, Akber R, Heijnis H. Vertical distributions of ^{210}Pb excess, ^7Be and ^{137}Cs in selected grass covered soils in Southeast Queensland, Australia. *Journal of Environmental Radioactivity*. 2006;**87**(2):135-147. DOI: 10.1016/j.jenvrad.2005.11.005

[24] Schuller P, Ellies A, Kirchner G. Vertical migration of fallout ^{137}Cs in agricultural soils from southern Chile. *Science of the Total Environment*. 1997;**193**(3):197-205. DOI: 10.1016/S0048-9697(96)05338-7

[25] Ramzaev V, Barkovsky A. Vertical distribution of ^{137}Cs in grassland soils disturbed by moles (*Talpa europaea* L.). *Journal of Environmental Radioactivity*. 2018;**184-185**:101-108. DOI: 10.1016/j.jenvrad.2018.01.011

[26] Mabit L, Bernard C. Relationship between soil ^{137}Cs inventories and chemical properties in a small intensively cropped watershed. *Comptes Rendus de l'Académie des Sciences-Serie IIA-Earth and Planetary Science*. 1998;**327**(8):527-532. DOI: 10.1016/S1251-8050(99)80034-2

[27] Ritchie JC, McCarty GW, Venteris ER, Kaspar TC. Soil and soil organic carbon redistribution on the landscape. *Geomorphology*. 2007;**89**:163-171. DOI: 10.1016/j.geomorph.2006.07.021

[28] Li X, McCarty GW, Karlen DL, Cambardella CA. Topographic metric

predictions of soil redistribution and organic carbon in Iowa cropland fields. *Catena*. 2018;**160**:222-232. DOI: 10.1016/j.catena.2017.09.026

[29] Li X, McCarty GW, Karlen DL, Cambardella CA, Effland W. Soil organic carbon and isotope composition response to topography and erosion in Iowa. *Journal of Geophysical Research – Biogeosciences*. 2018;**123**:3649-3667. DOI: 10.1029/2018JG004824

[30] Young CJ, Liu S, Schumacher JA, Schumacher TE, Kaspar TC, McCarty GW, et al. Evaluation of a model framework to estimate soil and soil organic carbon redistribution by water and tillage using ^{137}Cs in two U.S. Midwest agricultural fields. *Geoderma*. 2014;**232**:437-448. DOI: 10.1016/j.geoderma.2014.05.019

[31] Alewell C, Meusburger K, Juretzko G, Mabit L, Ketterer ME. Suitability of $^{239+240}\text{Pu}$ and ^{137}Cs as tracers for soil erosion assessment in mountain grasslands. *Chemosphere*. 2014;**103**:274-280. DOI: 10.1016/j.chemosphere.2013.12.016

[32] Mabit L, Benmansour M, Abril JM, Walling DE, Meusburger K, Iurian AR, et al. Fallout ^{210}Pb as a soil and sediment tracer in catchment sediment budget investigations: A review. *Earth-Science Reviews*. 2014;**138**:335-351. DOI: 10.1016/j.earscirev.2014.06.007

[33] Agapkina GI, Tikhomirov FA, Shcheglov AI, Kracke W, Bunzl K. Association of Chernobyl-derived Pu-239+240, Am-241, Sr-90 and Cs-137 with organic matter in the soil solution. *Journal of Environmental Radioactivity*. 1995;**29**(3):257-269. DOI: 10.1016/0265-931x(95)00023-4

[34] Van Pelt RS, Ketterer ME. Use of anthropogenic radioisotopes to estimate rates of soil redistribution by wind II: The potential for future use of $^{239+240}\text{Pu}$.

Aeolian Research. 2013;**9**:103-110. DOI: 10.1016/j.aeolia.2013.01.004

[35] Arata L, Alewell C, Frenkel E, A'Campo-Neuen A, Iurian AR, Ketterer ME, et al. Modelling deposition and erosion rates with RadioNuclides (MODERN)—Part 2: A comparison of different models to convert $^{239+240}\text{Pu}$ inventories into soil redistribution rates at unploughed sites. *Journal of Environmental Radioactivity*. 2016;**162-163**:97-106. DOI: 10.1016/j.jenvrad.2016.05.009

[36] Calitri F, Sommer M, Norton K, Temme A, Brandová D, Portes R, et al. Tracing the temporal evolution of soil redistribution rates in an agricultural landscape using $^{239+240}\text{Pu}$ and ^{10}Be . *Earth Surface Processes and Landforms*. 2019;**44**:1783-1798. DOI: 10.1002/esp.4612

[37] Schimmack W, Auerswald K, Bunzl K. Estimation of soil erosion and deposition rates at an agricultural site in Bavaria, Germany, as derived from fallout radiocesium and plutonium as tracers. *Die Naturwissenschaften*. 2002;**89**(1):43-46. DOI: 10.1007/s00114-001-0281-z

[38] Alewell C, Pitois A, Meusburger K, Ketterer M, Mabit L. $^{239+240}\text{Pu}$ from “contaminant” to soil erosion tracer: Where do we stand? *Earth-Science Reviews*. 2017;**172**:107-123. DOI: 10.1016/j.earscirev.2017.07.009

[39] Schimmack W, Auerswald K, Bunzl K. Can $^{239+240}\text{Pu}$ replace ^{137}Cs as an erosion tracer in agricultural landscapes contaminated with Chernobyl fallout? *Journal of Environmental Radioactivity*. 2001;**53**(1):41-57. DOI: 10.1016/S0265-931X(00)00117-X

[40] Meusburger K, Mabit L, Ketterer M, Park JH, Sandor T, Porto P, et al. A multi-radionuclide approach to evaluate the suitability of $^{239+240}\text{Pu}$ as soil erosion tracer. *Science of the Total*

Environment. 2016;**566-567**:1489-1499.
 DOI: 10.1016/j.scitotenv.2016.06.035

[41] Walling DE, He Q, Blake W. Use of ^7Be and ^{137}Cs measurements to document short- and medium-term rates of water-induced soil erosion on agricultural land. *Water Resources Research*. 1999;**35**(12):3865-3874

[42] Wallbrink PJ, Murray AS. Distribution and variability of ^7Be in soils under different surface cover conditions and its potential for describing soil redistribution processes. *Water Resources Research*. 1996;**32**(2):467-476. DOI: 10.1029/95WR02973

[43] Sepulveda A, Schuller P, Walling DE, Castillo A. Use of ^7Be to document soil erosion associated with a short period of extreme rainfall. *Journal of Environmental Radioactivity*. 2008;**99**(1):35-49. DOI: 10.1016/j.jenvrad.2007.06.010

[44] Walling DE, Schuller P, Zhang Y, Iroumé A. Extending the timescale for using Beryllium 7 measurements to document soil redistribution by erosion. *Water Resources Research*. 2009;**45**(2):1-13. DOI: 10.1029/2008WR007143

[45] Hancock GJ, Wilkinson SN, Hawdon AA, Keen RJ. Use of fallout tracers ^7Be , ^{210}Pb and ^{137}Cs to distinguish the form of sub-surface soil erosion delivering sediment to rivers in large catchments. *Hydrological Processes*. 2014;**28**(12):3855-3874. DOI: 10.1002/hyp.9926

[46] Matisoff G, Bonniwell EC, Whiting PJ. Soil erosion and sediment sources in an Ohio watershed using Beryllium-7, Cesium-137, and Lead-210. *Journal of Environmental Quality*. 2014;**31**(1):54-61. DOI: 10.2134/jeq2002.5400

[47] Ryken N, Vanden Nest T, Al-Barri B, Blake W, Taylor A, Bodé S, et al. Soil

erosion rates under different tillage practices in Central Belgium: New perspectives from a combined approach of rainfall simulations and ^7Be measurements. *Soil and Tillage Research*. 2018;**179**:29-37. DOI: 10.1016/j.still.2018.01.010

[48] Li Y, Yu H, Chappell A, Zhou N, Funk R. How much soil organic carbon sequestration is due to conservation agriculture reducing soil erosion? *Soil Research*. 2014;**52**(7):717-726. DOI: 10.1071/sr14078

[49] Whiting PJ, Matisoff G, Fornes W, Soster FM. Suspended sediment sources and transport distances in the Yellowstone River basin. *Geological Society of America Bulletin*. 2005;**117**(3-4):515-529. DOI: 10.1130/B25623.1

[50] Wallbrink PJ, Murray AS, Olley JM. Determining sources and transit times of suspended sediment in the Murrumbidgee River, New South Wales, Australia, using fallout ^{137}Cs and ^{210}Pb . *Water Resources Research*. 1998;**34**(4):879-887

[51] Wieder RK. Past, present, and future peatland carbon balance: An empirical model based on ^{210}Pb -dated cores. *Ecological Applications*. 2006;**11**(2):327-342. DOI: 10.2307/3060892

[52] Braakhekke MC, Wutzler T, Beer C, Kattge J, Schrumpf M, Ahrens B, et al. Modeling the vertical soil organic matter profile using Bayesian parameter estimation. *Biogeosciences*. 2013;**10**(1):399-420. DOI: 10.5194/bg-10-399-2013

[53] Teramage MT, Onda Y, Kato H, Wakiyama Y, Mizugaki S, Hiramatsu S. The relationship of soil organic carbon to ^{210}Pb and ^{137}Cs during surface soil erosion in a hillslope forested environment. *Geoderma*. 2013;**192**(1):59-67. DOI: 10.1016/j.geoderma.2012.08.030

- [54] Dörr H, Münnich KO. Downward movement of soil organic matter and its influence on trace-element transport (^{210}Pb , ^{137}Cs) in the soil. *Radiocarbon*. 1989;**31**(3):655-663. DOI: 10.1017/s003382220001225x
- [55] Follett RF, Kimble J, Leavitt SW, Pruessner E. Potential use of soil C isotope analyses to evaluate paleoclimate. *Soil Science*. 2004;**169**(7):471-488. DOI: 10.1097/01.ss.0000135169.45251.63
- [56] Fox JF, Papanicolaou AN. The use of carbon and nitrogen isotopes to study watershed erosion processes. *Journal of the American Water Resources Association*. 2007;**43**(4):1047-1064. DOI: 10.1111/j.1752-1688.2007.00087.x
- [57] Hancock G, Revill A. Land-Use and Erosion Source Discrimination of Soil and Carbon Sources to the Logan and Albert Rivers Using Compound Specific Isotope Analysis [Internet]. 2011. Available from: <https://pdfs.semanticscholar.org/5d40/96f85df226994a0f4e990f46e088ed89f188.pdf>
- [58] Paul EA, Follett RF, Leavitt SW, Halvorson A, Peterson GA, Lyon DJ. Radiocarbon dating for determination of soil organic matter pool sizes and dynamics. *Soil Science Society of America Journal*. 1997;**61**:1058-1067
- [59] Bowen GJ. Isoscapes: Spatial pattern in isotopic biogeochemistry. *Annual Review of Earth and Planetary Sciences*. 2010;**38**:161-187. DOI: 10.1146/annurev-earth-040809-152429
- [60] West JB, Sobek A, Ehleringer JR. A simplified GIS approach to modeling global leaf water isoscapes. *PLoS One*. 2008;**3**(6):e2447. DOI: 10.1371/journal.pone.0002447. Chave J, editor
- [61] West JB, Bowen GJ, Dawson TE, Tu KP. Understanding Movement, Pattern, and Process, on Earth through Isotope Mapping. Dordrecht/Heidelberg/London/New York: Springer; 2009. 487p
- [62] Powell RL, Yoo E-H, Still CJ. Vegetation and soil Carbon-13 isoscapes for South America: Integrating remote sensing and ecosystem isotope measurements. *Ecosphere*. 2012;**3**(11):109. DOI: 10.1890/es12-00162.1
- [63] Li QY, Fang HY, Sun LY, Cai QG. Using the ^{137}Cs technique to study the effect of soil redistribution on soil organic carbon and total nitrogen stocks in an agricultural catchment of Northeast China. *Land Degradation & Development*. 2014;**25**(4):350-359. DOI: 10.1002/ldr.2144
- [64] Quijano L, Gaspar L, Navas A. Spatial patterns of SOC, SON, ^{137}Cs and soil properties as affected by redistribution processes in a Mediterranean cultivated field (Central Ebro Basin). *Soil and Tillage Research*. 2016;**155**:318-328. DOI: 10.1016/j.still.2015.09.007
- [65] Ladd B, Peri PL, Pepper DA, Silva LCR, Sheil D, Bonser SP, et al. Carbon isotopic signatures of soil organic matter correlate with leaf area index across woody biomes. *Journal of Ecology*. 2014;**102**(6):1606-1611. DOI: 10.1111/1365-2745.12309
- [66] Walling DE, Zhang Y, He Q. Models for deriving estimates of erosion and deposition rates from fallout radionuclide (Caesium-137, excess Lead-210, and Beryllium-7) measurements and the development of user friendly software for model implementation. In: *Impact of Soil Conservation Measures on Erosion Control and Soil Quality*. Vienna; IAEA-TECDOC-1665; 2011. pp. 11-33
- [67] Conrad O, Bechtel B, Bock M, Dietrich H, Fischer E, Gerlitz L, et al. System for automated geoscientific analyses (SAGA) v. 2.1.4. *Geoscientific Model Development*. 2015;**8**:1991-2007. DOI: 10.5194/gmd-8-1991-2015

- [68] Li X, McCarty GW. Use of principal components for scaling up topographic models to map soil redistribution and soil organic carbon. *Journal of Visualized Experiments*. 2018;**140**:e58189. DOI: 10.3791/58189
- [75] Van Oost K, Govers G, de Alba S, Quine TA. Tillage erosion: A review of controlling factors and implications for soil quality. *Progress in Physical Geography*. 2006;**30**(4):443-466. DOI: 10.1191/0309133306pp487ra
- [69] Moriasi DN, Arnold JG, Van Liew MW, Binger RL, Harmel RD, Veith TL. Model evaluation guidelines for systematic quantification of accuracy in watershed simulations. *Transactions of the ASABE*. 2007;**50**(3):885-900. DOI: 10.13031/2013.23153
- [70] Throne M. Southern Iowa agriculture, 1833-1890: The progress from subsistence to commercial corn-belt farming. *Agricultural History Society*. 1949;**23**:124-130. DOI: 10.2307/3740927
- [71] Broder MW, Wagner GH. Microbial colonization and decomposition of corn, wheat, and soybean residue. *Soil Science Society of America Journal*. 1988;**52**(1): 112-117. DOI: 10.2136/sssaj1988.03615995005200010020x
- [72] Li X, McCarty GW. Application of topographic analyses for mapping spatial patterns of soil properties. In: Pepe A, editor. *Earth Observation and Geospatial Analyses Geometry*. London: IntechOpen; 2019. pp. 1-32. DOI: 10.5772/57353
- [73] Dormann CF, Elith J, Bacher S, Buchmann C, Carl G, Carré G, et al. Collinearity: A review of methods to deal with it and a simulation study evaluating their performance. *Ecography*. 2013;**36**(1):027-046. DOI: 10.1111/j.1600-0587.2012.07348.x
- [74] Heckrath G, Djurhuus J, Quine TA, Van Oost K, Govers G, Zhang Y. Tillage erosion and its effect on soil properties and crop yield in Denmark. *Journal of Environmental Quality*. 2005;**34**:312-324. DOI: 10.1029/2002GB002010